Temporal and Spatial Interference between Four-Wave Mixing and Six-Wave Mixing Channels

Yanpeng Zhang,[1,2,*] Utsab Khadka,[1] Blake Anderson,[1] and Min Xiao[1,†]

[1]*Department of Physics, University of Arkansas, Fayetteville, Arkansas 72701, USA*

[2]*Key Laboratory for Physical Electronics and Devices of the Ministry of Education, Xi'an Jiaotong University, Xi'an 710049, China*

(Received 20 July 2008; published 7 January 2009)

Using phase control between four-wave mixing (FWM) and six-wave mixing (SWM) channels in a four-level atomic system, we demonstrate temporal and spatial interferences between these two nonlinear optical processes. Efficient and coexisting FWM and SWM signals are produced in the same electromagnetically induced transparency window via atomic coherence. The temporal interference has a femtosecond time scale corresponding to the optical transition frequency. Such studies of intermixing between different order nonlinear optical processes with a controllable phase delay can have important applications in high-precision measurements, coherence quantum control, and quantum information processing.

DOI: 10.1103/PhysRevLett.102.013601 PACS numbers: 42.50.Gy, 42.25.Hz, 42.65.−k

When two transition paths exist between an initial state and a final state, the total transition probability can be either enhanced or suppressed, depending on the relative phase between the two transition amplitudes [1–6]. Such a quantum coherent control technique has been used to control the transition probability in atoms [1], photoelectron angular distribution [6], phase-controlled current in semiconductors [2], and various chemical reactions [4,7,8]. Also, a fifth-order time-frequency Raman spectroscopy technique was used to study the two-quantum transition or Raman overtone for the rephasing pathway [9].

In this Letter, we experimentally demonstrate a new type of phase-controlled, spatiotemporal coherent interference between four-wave-mixing (FWM) and six-wave-mixing (SWM) processes in a four-level, inverted-Y system in rubidium atoms. By making use of atomic coherence induced by laser fields among different energy levels, the SWM signal can be greatly enhanced and even made to be in the same order of magnitude as the coexisting FWM signal [10,11]. With a specially designed spatial configuration for the laser beams for phase matching and an appropriate optical delay introduced in one of the pump laser beams, we can have a controllable phase difference between the dominant FWM and SWM processes in the system. When this relative phase is varied, temporal, as well as spatial, interferences can be observed. The interference in the time domain is in the femtosecond time scale, corresponding to the optical transition frequency excited by the delayed pump laser beam. The current experiment is done with weak cw lights interacting with near-resonant atomic transitions, which is quite different from the earlier works of fifth-order time-frequency Raman spectroscopy used to study liquids or solution phase dynamics [9]. Understanding the mechanism for efficient generations of high-order nonlinear optical processes and interplays between them, especially with the ability to control these processes with a controllable phase difference, can have broad impacts in many fields of science including coherent control for chemical reactions [4,7,8], stable 2D-soliton generation for optical communications [12], high-precision spectroscopy [13], nonlinear spectroscopy [9], stabilization and compression of high-intensity optical pulses in cubic-quintic nonlinear media, and quantum information processing [14,15].

Let us consider a four-level inverted Y-type atomic system as shown in Fig. 1(b). The four relevant energy levels are $5S_{1/2}$, $F = 2$ ($|0\rangle$), $5S_{1/2}$, $F = 3$ ($|3\rangle$), $5P_{3/2}$ ($|1\rangle$), and $5D_{5/2}$ ($|2\rangle$) in ^{85}Rb. In the three-level ladder-type subsystem ($|0\rangle - |1\rangle - |2\rangle$), as shown in Fig. 1(a), if a strong coupling beam E_2 (frequency ω_2, $\mathbf{k}_2$, and Rabi frequency G_2) couples to the upper transition and a weak probe beam E_1 (frequency ω_1, $\mathbf{k}_1$, and Rabi frequency G_1) interacts with the lower transition, and they propagate in the opposite direction through the atomic medium, an electromagnetically induced transparency (EIT) window will be created for the probe field due to the two-photon, Doppler-free configuration in this Doppler-broadened atomic medium [16]. When another coupling laser beam E_2' (frequency ω_2, $\mathbf{k}_2'$, and G_2') is also applied to the upper transition [Fig. 1(a)], a FWM signal will be generated with frequency ω_1 in the created EIT window of the ladder subsystem. Such FWM (E_F) process can be described by using a perturbative chain: $\rho_{00}^{(0)} \to^{\omega_1} \rho_{10}^{(1)} \to^{\omega_2} \rho_{20}^{(2)} \to^{-\omega_2} \rho_{10}^{(3)}$ [10]. If we align the coupling and probe laser beams in a spatial pattern, as shown in Fig. 1(c), the generated FWM signal (E_F) will have a small angle θ from $\mathbf{k}_1$, satisfying the phase-matching condition $\mathbf{k}_F = \mathbf{k}_1 + \mathbf{k}_2 - \mathbf{k}_2'$. The FWM efficiency depends on the intensities of all the laser beams involved. Next, let us turn our attention to Fig. 1(b), where coupling beam E_2' is blocked and two pump beams E_3 (ω_3, $\mathbf{k}_3$, and G_3) and E_3' (ω_3, $\mathbf{k}_3'$, and G_3') are applied on transition $|3\rangle - |1\rangle$. The laser beams are carefully aligned in the square-box pattern [10], as shown in Fig. 1(c). In this case, the FWM channel in the ladder subsystem is turned off (without E_2'), and the FWM process in the $\wedge$-type subsystem ($|0\rangle - |1\rangle - |3\rangle$) is not efficient (not observable

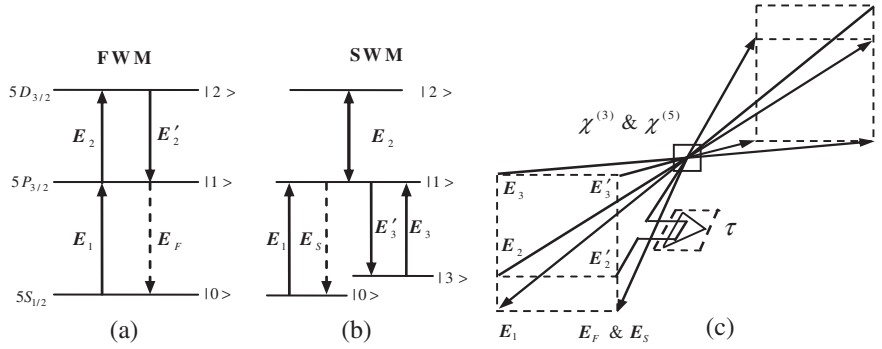

FIG. 1. Atomic levels and laser beam arrangements for generating coexisting FWM (a) and SWM (b) processes in the same EIT window. The dash-dotted lines are the generated FWM (E_F) and SWM (E_S) signals. (c) Spatial beam (square-box) geometry used in the experiment, τ is a time delay through a precision translation stage for beam E_2'.

in the experiment) since no EIT window exists for this configuration (the probe and pump beams counter-propagate) [16]. From phase-matching condition ($\mathbf{k}_S = \mathbf{k}_1 + \mathbf{k}_3 - \mathbf{k}_3' + \mathbf{k}_2 - \mathbf{k}_2$), efficient SWM signals can be generated via either $\rho_{00}^{(0)} \rightarrow^{\omega_1} \rho_{10}^{(1)} \rightarrow^{\omega_2} \rho_{20}^{(2)} \rightarrow^{-\omega_2} \rho_{10}^{(3)} \rightarrow^{-\omega_3} \rho_{30}^{(4)} \rightarrow^{\omega_3} \rho_{10}^{(5)}$ or $\rho_{00}^{(0)} \rightarrow^{\omega_1} \rho_{10}^{(1)} \rightarrow^{-\omega_3} \rho_{30}^{(2)} \rightarrow^{\omega_3} \rho_{10}^{(3)} \rightarrow^{\omega_2} \rho_{20}^{(4)} \rightarrow^{-\omega_2} \rho_{10}^{(5)}$, which are both in the direction of θ angle from $\mathbf{k}_1$ [denoted as $\mathbf{k}_S$ and E_S with frequency ω_1 in Figs. 1(b) and 1(c)], and these SWM signals also fall into the same EIT window as the FWM signal in the ladder subsystem. In the generated FWM and SWM signal beams, the coherence lengths are given by $l_F = 2c/[n(\omega_2/\omega_1)|\omega_2 - \omega_1|\theta^2]$ and $l_S = 2c/[n(\omega_3/\omega_1)|\omega_3 - \omega_1|\theta^2]$, respectively, with n being the refractive index at the frequency ω_1. In the experiment, θ is very small (0.3°) so that l_F and l_S are much larger than the interaction length L, so the phase-mismatch effect can be neglected.

Now, we add the coupling beam E_2' back into the upper transition, but keep its power to be adjustable. When the power of E_2' is same as the power of E_2, the FWM process in the ladder subsystem is very efficient and it dominates over the SWM processes, typically larger by several orders of magnitude [17]. However, as the power of E_2' decreases, the FWM signal reduces rapidly and the relative strengths of the SWM signals increase, until the SWM signals dominate when E_2' is reduced to near zero. By carefully adjusting the power of E_2' relative to E_2, the SWM signals are made to be in the same strength as the FWM signal, as shown in Fig. 2(a), and both fall in the same EIT window [Fig. 2(b)]. Since $G_2' \ll G_2$ when SWM signals get to be the same order as the FWM, the SWM processes with E_2' replacing E_2 in Fig. 1(b) can be negligible. Notice that E_2' is only involved in the FWM process, so it can be used to tune not only the relative strength of the FWM and SWM processes, but also the relative phase between these two nonlinear wave-mixing processes.

The experiment was done with ^{85}Rb atoms in an atomic vapor cell of 5 cm long, which is wrapped in μ-metal for magnetic shielding and heated to 60 °C. The probe beam E_1 is from an extended-cavity diode laser (ECDL) at 780.23 nm. The coupling beams E_2 and E_2' are split from another ECDL at 775.98 nm. The beam E_2' is delayed by an amount τ using a computer-controlled stage. The pump beams E_3 and E_3' are split from a cw Ti:sapphire laser at 780.24 nm. The CCD and an avalanche photodiode (APD) are set at an angle θ from the probe beam (with a beam splitter) to measure the dominant FWM and SWM signals. The transmitted probe beam is simultaneously monitored by a silicon photodiode. The power and frequency detuning of the coupling beam E_2 (E_2') are 40 mW (4 mW) and 170 MHz, and those of the pump beam E_3 ($=E_3'$) are 67 mW and 0 MHz, respectively. Under the conditions of $G_3, G_3' > G_2 \gg G_2', G_1$, and neglecting other multi-wave mixing processes either very weak or propagating in other directions, the total detected intensity at angle θ is given by the coexisting FWM (E_F) and SWM (E_S) signals as

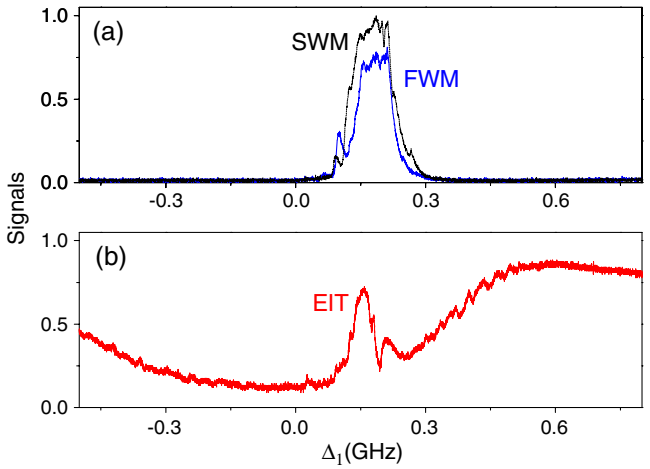

FIG. 2 (color online). (a) Measured EIT-assisted FWM (solid line) and SWM (dashed line) signal intensities; (b) Corresponding probe beam transmission versus probe detuning Δ_1. The experimental parameters are $G_1 = 2\pi \times 15$ MHz, $G_2 = 2\pi \times 60$ MHz, $G_2' = 2\pi \times 19$ MHz, $G_3 = G_3' = 2\pi \times 87$ MHz, $\Delta_3 = 0$, and $\Delta_2 = 170$ MHz.

$$I(\tau, r) \propto |\chi^{(3)}|^2 + |\eta\chi^{(5)}|^2 + 2\eta|\chi^{(3)}||\chi^{(5)}|\cos(\varphi_3 - \varphi_5 + \varphi), \quad (1)$$

where $\eta = \varepsilon_2\varepsilon_3\varepsilon_3'/\varepsilon_2'$, $\chi^{(3)} = -i\mu_1^2\mu_2^2N/\{\varepsilon_0\hbar^3 d_1 d_2[d_1 + (G_3 + G_3')^2/d_3]\} = |\chi^{(3)}|\exp(i\varphi_3)$, $\chi^{(5)} = 2i\mu_1^2\mu_2^2\mu_3^2N/(\varepsilon_0\hbar^5 d_1^3 d_2 d_3) = |\chi^{(5)}|\exp(i\varphi_5)$, $d_1 = \Gamma_{10} + i\Delta_1$, $d_2 = \Gamma_{20} + i(\Delta_1 + \Delta_2)$, $d_3 = \Gamma_{30} + i(\Delta_1 - \Delta_3)$ with $\Delta_i = \Omega_i - \omega_i$, $\varphi = \Delta\mathbf{k}\cdot\mathbf{r} - \omega_2\tau$, and $\Delta\mathbf{k} = \mathbf{k}_F - \mathbf{k}_S = (\mathbf{k}_2 - \mathbf{k}_2') - (\mathbf{k}_3 - \mathbf{k}_3')$. μ_1, μ_2, and μ_3 are the dipole moments of the transitions $|0\rangle - |1\rangle$, $|1\rangle - |2\rangle$, and $|3\rangle - |1\rangle$, respectively, and ε_2, ε_2', ε_3, ε_3' are the respective amplitudes of the fields. The nonlinear phase φ_3 and φ_5 depend on the atomic parameters (such as Γ_{i0} and Δ_i), so for a given set of experimental parameters the nonlinear phase difference in Eq. (1) determines the initial phase for the interference fringe.

From Eq. (1), it is clear that the total signal has not only spatial interference with a period of $2\pi/\Delta k$, but also an ultrafast time oscillation with a period of $2\pi/\omega_2$, which form a spatiotemporal interferogram. With a plane-wave approximation and the square-box configuration for the laser beams [Fig. 1(c)], the spatial interference occurs in the plane perpendicular to the propagation direction. Figure 3 depicts a typical three-dimensional interferogram pattern [Fig. 3(a)] and its projections on time [Fig. 3(c)] and space [Fig. 3(d)] planes, respectively. Figure 3(b) presents a theoretical simulation for the total intensity with appropriate parameters. The temporal oscillation period is measured to be $2\pi/\omega_2 = 2.588$ fs, which corresponds to the $5P_{3/2}$ to $5D_{5/2}$ transition frequency of $\Omega_2 = 2.427$ fs^{-1} in ^{85}Rb. Such measurement of atomic transition frequency in optical wavelength range is Doppler free and can be used as a technique for precision frequency measurement. The spatial interference is determined by $\Delta k \approx 2\pi|\lambda_2 - \lambda_3|\theta/\lambda_2\lambda_3$. In our experimental situation, we have $2\pi/\Delta k = 3.3$ mm along the direction of $\Delta\mathbf{k}$, which gives a little more than one interference fringe, as shown in Fig. 3(d). When the phase delay is varied on E_2' beam, the spatial interference pattern can be changed from destructive to constructive at the center of the beam profile ($r = 0$) [18]. The solid curves in Fig. 3(c) and 3(d) are theoretical calculations from the full density-matrix equations, which fit well with the experimentally measured results.

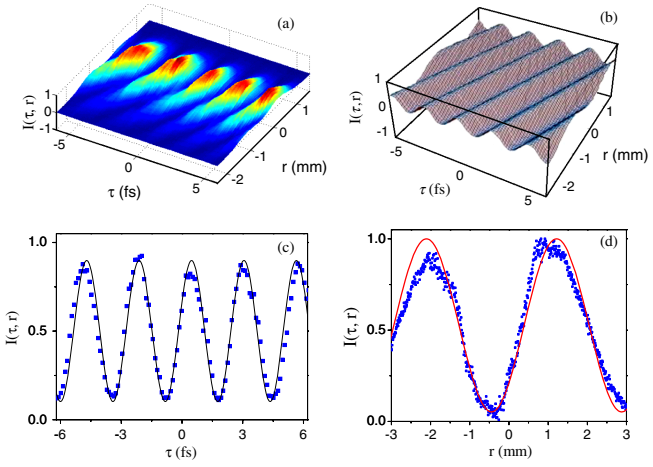

FIG. 3 (color online). (a) A three-dimensional spatiotemporal interferogram of the total FWM + SWM signal intensity $I(\tau, r)$ versus time-delay τ and transverse position r. (b) The theoretically simulated result from Eq. (1). (c) Cross section of spatiotemporal interferogram on time plane ($r = 0$) (square points are experimental data, and the solid curve is the theoretically simulated result). (d) Measured (square points) and calculated (solid curve) cross sections of the spatiotemporal interferogram on space plane ($\tau = 0$). The signal intensity is normalized to 1. The parameters are $\Omega_2 = 2.427$ fs^{-1}, $\Delta k = 1.9$ mm^{-1}, and $\eta = 1.5$.

To see how well the transition frequency Ω_2 can be determined from such time interference fringe, we need to consider two cases. When the laser linewidths are much narrower than the homogeneous linewidths of the transitions, the phase fluctuations of the laser fields will limit the range of the time delay, which puts an upper bound on the accuracy of the modulation frequency measurement. In such case, the accuracy of measuring modulation frequency is determined by the laser linewidths. This measurement depends on how well ω_2 can be tuned to the transition frequency Ω_2, and is Doppler-free, which can be useful in optical spectroscopy and precision measurements. In the other case, when the laser bandwidths are larger than the atomic decay rates, the modulation frequency corresponds directly to the resonant frequency Ω_2. The accuracy in the modulation frequency measurement will then be determined by the homogeneous linewidths of the atomic transitions, even in the Doppler-broadened atomic medium, which is applicable to transitions between metastable states.

Figure 4(a) shows the temporal interference with a much longer time delay in beam E_2', which makes the spatiotemporal interferogram to be dominated by the temporal component. By fitting the interference fringe [Fig. 4(b)], the period is determined to be 2.588 fs. Using Fourier transformation of the interferogram data (with a time-delay change of 50 ps), as shown in Fig. 4(c), the modulation frequency is determined to be 2.427 ± 0.004 fs^{-1}, which corresponds to the resonant frequency of the transition from $5P_{3/2}$ to $5D_{5/2}$ in ^{85}Rb. Of course, what we present here is simply a proof of principle demonstration with laser linewidths of about 1 MHz and such measurement technique can surely be further improved.

A few points are worth mentioning here. First, our experimental results indicate that we can not only enhance SWM to be in the same order of strength as the coexisting FWM, but also manipulate their spatial and temporal behaviors by controlling the phase delay in one of the laser beams. Such spatiotemporal interferogram between FWM

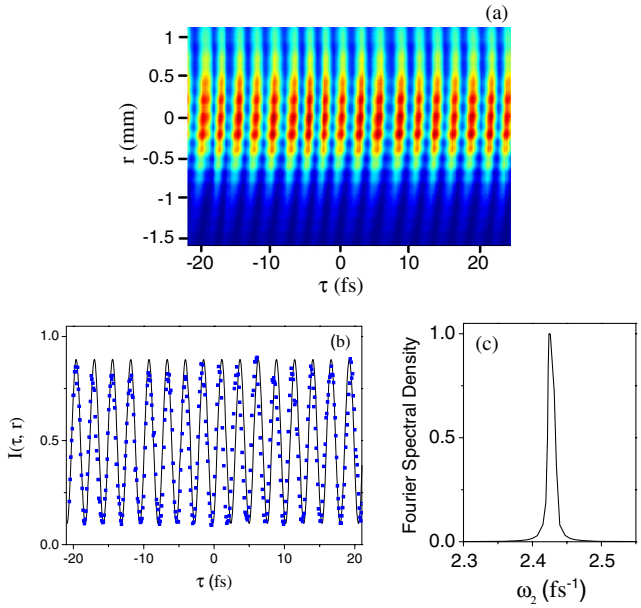

FIG. 4 (color online). (a) The spatiotemporal interferogram versus τ and r, $\Omega_2 = 2.427\ \mathrm{fs}^{-1}$, $\Delta k = 1.9\ \mathrm{mm}^{-1}$, and $\eta = 1.5$. (b) Measured beat signal (dot points) via delay time τ together with the theoretically simulated result (solid curve). (c) Fourier spectrum of the beat signal.

and SWM signals was generated with three independent laser sources. Second, by adjusting the power of the E_2' beam, the relative strengths of the FWM and SWM signals can be easily adjusted. In the case of making $E_S \ll E_F$ (letting $E_2' \rightarrow E_2$ in power), Eq. (1) can serve as a heterodyne detection method to determine the ratio of high-order nonlinear susceptibilities ($\chi^{(5)}/\chi^{(3)}$). Since $\chi^{(3)}$ can be easily measured [19], the $\chi^{(5)}$ coefficient in such atomic medium can then be determined. The subtle phase coherence control of $\varphi_3 + \varphi = 2n\pi$ and $(2n + 1/2)\pi$ can be employed to yield the real and imaginary parts of $\chi^{(5)}$, respectively. Third, the technique used here can be easily transferred to solid materials, in which EIT and FWM processes can be easily obtained. Fourth, with controlled FWM and SWM processes and their enhanced efficiencies via atomic coherence and the opened EIT window, three-photon entanglement or correlated triplet photons [14] can be generated for testing fundamental quantum mechanics and quantum information processing [14,15].

In summary, efficient FWM and SWM processes have been shown to coexist in the four-level inverted-Y atomic system. By adjusting the intensity and time delay of one of the coupling beams (E_2'), the relative strength and spatiotemporal interferences between the FWM and SWM channels can be controlled. The generated spatiotemporal interferogram in femtosecond time scale can be used to determine the optical transition frequency with a Doppler-free precision. Such manipulations of high-order nonlinear optical processes and their interplays in multilevel atomic systems can have potential applications in coherence quantum control, nonlinear optical spectroscopy, stabilization and compression of high-intensity optical pulses in such efficient cubic-quintic nonlinear media, precision measurements, and quantum information processing.

Funding support in part by the National Science Foundation is acknowledged.

*ypzhang@mail.xjtu.edu.cn
†mxiao@uark.edu

[1] C. Chen, Y. Yin, and D. S. Elliott, Phys. Rev. Lett. **64**, 507 (1990).
[2] E. Dupont *et al.*, Phys. Rev. Lett. **74**, 3596 (1995).
[3] L. Zhu, V. Kleiman, X. Li, S. P. Lu, K. Trentelman, and R. J. Gordon, Science **270**, 77 (1995).
[4] K. Ohmori, Y. Sato, E. E. Nikitin, and S. A. Rice, Phys. Rev. Lett. **91**, 243003 (2003).
[5] M. Gunawardena and D. S. Elliott, Phys. Rev. Lett. **98**, 043001 (2007).
[6] R. Yamazaki and D. S. Elliott, Phys. Rev. Lett. **98**, 053001 (2007).
[7] H. Rabitz, R. de Vivie-Riedle, M. Motzkus, and K. Kompa, Science **288**, 824 (2000).
[8] S. A. Rice and M. Zhan, *Optical Control of Molecular Dynamics* (Wiley, New York, 2000).
[9] K. J. Kubarych, C. J. Milne, and R. J. D. Miller, Int. Rev. Phys. Chem. **22**, 497 (2003); S. Saito and I. Ohmine, Phys. Rev. Lett. **88**, 207401 (2002); D. J. Ulness, J. C. Kirkwood, and A. C. Albrecht , J. Chem. Phys. **108**, 3897 (1998).
[10] Y. P. Zhang and M. Xiao, Appl. Phys. Lett. **90**, 111104 (2007).
[11] Y. P. Zhang, A. W. Brown, and M. Xiao, Phys. Rev. Lett. **99**, 123603 (2007).
[12] H. Michinel, M. J. Paz-Alonso, and V. M. Perez-Garcia, Phys. Rev. Lett. **96**, 023903 (2006).
[13] T. Udem, R. Holzwarth, and T. W. Hänsch, Nature (London) **416**, 233 (2002).
[14] J. M. Wen, S. G. Du, Y. P. Zhang, M. Xiao, and M. H. Rubin, Phys. Rev. A **77**, 033816 (2008).
[15] V. Boyer, A. M. Marino, R. C. Pooser, and P. D. Lett, Science **321**, 544 (2008).
[16] J. Gea-Banacloche, Y. Li, S. Jin, and M. Xiao, Phys. Rev. A **51**, 576 (1995).
[17] R. W. Boyd, *Nonlinear Optics* (Academic Press, New York, 1992).
[18] B. Anderson, Y. P. Zhang, U. Khadka, and Min Xiao, Opt. Lett. **33**, 2029 (2008).
[19] H. Wang, D. Goorskey, and M. Xiao, Phys. Rev. Lett. **87**, 073601 (2001).